LANGMUIR

pubs.acs.org/Langmuir Article

Optical Fibers Functionalized with Single-Walled Carbon Nanotubes for Flexible Fluorescent Catecholamine Detection

Madeline E. Klinger, Rigney A. Miller, Natsumi Komatsu, Amanda Shiu, Linda Wilbrecht, and Markita P. Landry*

Cite This: https://doi.org/10.1021/acs.langmuir.4c04910 Read Online

ACCESS | Metrics & More | Article Recommendations | Supporting Information

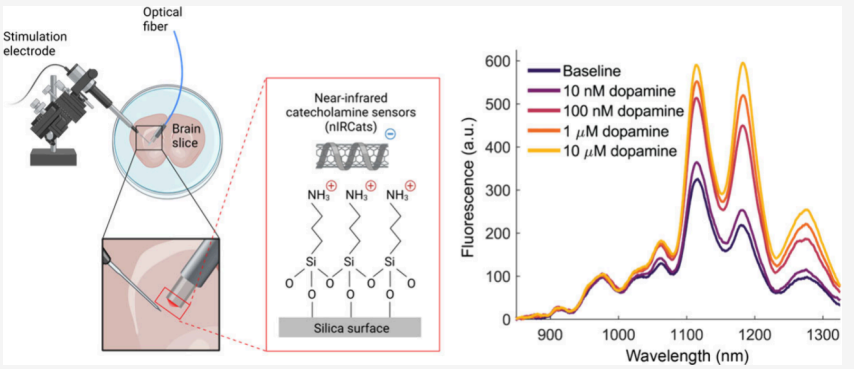

ABSTRACT: Despite the popularity of drugs that act on catecholamine receptors, our knowledge of catecholamine dynamics in human health and disease remains incomplete. Recent advances in fluorescent sensors have enabled unprecedented access to catecholamine dynamics in preclinical animal models, but the requirements of these technologies to use in model organisms limit their translational value for clinical diagnostics. Here, we introduce proof of principle fluorescent catecholamine detection via optical fibers functionalized with single-walled carbon nanotube (SWNT)-based near-infrared catecholamine sensors (nIRCats), a catecholamine detection form factor that has potential for more convenient and less invasive clinical translation. We show that these near-infrared functionalized (nIRF) fibers respond to dopamine in a biologically relevant concentration range (10 nM through 1 μM), with minimal responsivity loss following 16 h exposure to human blood plasma. We further demonstrate the utility of these fibers in detecting dopamine from as little as 10 μL volumes of clinically relevant biofluids up to 24 weeks after fiber synthesis. We also introduce a compact, mobile dual-near-infrared fiber photometry rig and demonstrate its success detecting dopamine in acute brain slices with nIRF fibers. Together, this fiber-based dopamine detection tool and photometry rig expand the toolset for catecholamine detection.

INTRODUCTION

The catecholamine dopamine has been implicated in movement and reward prediction,[1,2] neurodegenerative diseases such as Parkinson's and Alzheimer's Diseases,[3,4] neuropsychiatric disorders,[5] and physiological functions.[6−9] Dopamine is hydroxylated to norepinephrine (noradrenaline), which is similarly implicated in neurological and psychiatric illness,[10−12] stress and arousal,[13] memory,[14] and other functions.[15] While the last few decades of research have demonstrated interactions between dopamine and norepinephrine in health and disease,[10,11,16−19] our understanding is far from complete, and physicians have limited tools to monitor catecholamine levels in human patients.[20] To accelerate this field of study, versatile technologies to examine catecholamine dynamics are needed that can function in settings from preclinical animal models to human patients.

In recent years, nongenetically encoded fluorescent molecules have emerged as viable tools for bioimaging both *ex vivo* and *in vivo*. In particular, single-walled carbon nanotubes (SWNTs) have demonstrated remarkable flexibility as biocompatible biosensors, capable of detecting DNA polymorphisms, nitric oxide, proteins, and other biomarkers.[21−23] These sensors rely on the intrinsic near-infrared (nIR) fluorescence of SWNTs, which can be modulated by adsorbed polymers to increase emission in the presence of select analytes. Functionalized SWNTs emit at 1000−1300 nm, well within the nIR-II "second window" of optimal biological imaging, in which tissue absorbance and scattering of photons

Received: December 3, 2024
Revised: March 31, 2025
Accepted: March 31, 2025

is minimal.[24] Functionalized SWNTs employed in drug delivery investigations have demonstrated low toxicity *in vivo*.[25] Examination of blood serum biomarkers in rodents after intravenous injection of DNA-functionalized SWNTs suggests long-term (~5 months) biocompatibility,[26] and implanted SWNT-based chemical sensors have previously been used to measure nitric oxide in mice for over 400 days.[27] These features position SWNT-based biosensors as a promising candidate for long-term biological *ex vivo* and *in vivo* imaging, where their synthetic nature facilitates easy adoption for use across animal species.

As a proof of concept, we here leverage the functional properties of SWNTs to develop optical fibers surface-functionalized with near-infrared catecholamine nanosensors (nIRCats) for rapid detection of catecholamines in small volumes of biofluids, permitting reuse of both fibers and biofluid samples. nIRCats are SWNTs functionalized with $(GT)_6$ single-stranded DNA that emit up to a 24-fold and 35-fold increase in fluorescence ($\Delta F/F_0$) in response to dopamine and norepinephrine, respectively, *in vitro*.[28] To date, we have validated the use of nIRCats in solution for measuring evoked dopamine release in *ex vivo* striatal brain tissue with micron-level spatial resolution and millisecond-level temporal resolution, in the presence of pharmacological agents, and in evaluating Huntington's Disease progression.[28,29] nIRCats immobilized on glass surfaces have also been used to measure neuronal dopamine signaling on a subcellular scale.[30,31] Immobilizing nIRCats on optical fibers couples our catecholamine-sensing technology with fiber photometry, a commonly employed method in systems and behavioral neuroscience, thus expanding the conceptual imaging toolkit to permit a more adaptable experimental paradigm for a wider variety of applications. While SWNT-based sensors have previously been coupled to fiber optics using an intermediate hydrogel,[32] the scale of that particular form factor precludes potential use in animal research. Our approach thus presents novel utility, both in terms of scale and in terms of the direct coupling between the silica fiber and sensor. Using these nIRCat-functionalized optical (nIRF) fibers, we demonstrate a fluorescent response to 10 nM dopamine in as little as 10 μL biofluid *in vitro* and record endogenous dopamine transients evoked by electrical stimulation in *ex vivo* mouse brain tissue. We show that nIRF fibers are shelf-stable for 24 weeks postsynthesis, reusable, and nonbiofouling in human plasma. Together, these results suggest translatable potential for real-time readout of catecholamine release in biological environments.

EXPERIMENTAL SECTION

Fiber Preparation (Standard). Aminosilanes are a class of compounds commonly used as coupling agents for silica-based materials such as glass. In solution, the amine groups interact with negatively charged molecules, such as DNA. We leveraged this interaction to develop an aminosilane-based protocol, loosely based on previous demonstrations of silica silanization,[33] to immobilize nIRCats on glass optical fibers for photometric measurement of dopamine. We used a 400 μm-diameter core multimode silica optical fiber (Thorlabs FP400URT, 0.5 NA) glued with epoxy into a 1.25 mm diameter iron ferrule (Thorlabs SFLC440). The exposed length of fiber was trimmed to 4.5 mm, the approximate depth of the rodent nucleus accumbens from the brain surface. Fibers were first cleaned by immersion for at least 5 min each in acetone, isopropyl alcohol, and molecular grade water, in that order.

Hydroxylation of Silica Surface. This procedure was incorporated only for data represented in Figure 3. Fibers were soaked in potassium permanganate solution for 30 min, washed repeatedly with water, soaked in a solution of potassium hydroxide in ethanol for 30 min, again washed with water, then placed in a glass vial which had been pretreated with piranha solution (1:1 (v/v) concentrated sulfuric acid and 30% hydrogen peroxide). 300 μL fresh piranha solution was added to the vial and fibers were incubated for 30 min. Fibers were then washed with water to remove ionic debris, ethanol to remove water and less polar contaminants, and toluene to remove ethanol.

Silanization. Prepared fibers were placed in an oven-dried 3-necked round-bottom flask containing 19 mL anhydrous toluene. The flask was connected to a condenser and continuously flushed with nitrogen gas. Exposed flask necks were secured with septa, and 1 mL (3-Aminopropyl)triethoxysilane (APTES, 99%, Sigma-Aldrich) was injected through one neck to create a 5% APTES solution in toluene. To increase APTES-silica hydrolyses and minimize APTES polymerization, we aimed to attenuate atmospheric humidity. The flask was then lowered into an 80 °C heated oil bath and the condenser was flushed with cold tap water to reduce evaporate throughout the 1 h silanization reaction.

Functionalization with nIRCats. Postsilanization, tips were immersed for at least 5 min each in toluene, ethanol, and molecular grade water, in that order, to displace any residual weakly bonded silanes. Fibers were then dried overnight in a 110 °C oven to promote formation of siloxane bonds. Afterward, fibers were incubated in 50−200 mg/L nIRCats solution (manufactured in-house as in Beyene et al., 2019) for 30−60 min. Fibers were passively incubated or incubated with bath sonication for 30 min followed by a rest of at least 30 min. Immediately after nIRCats incubation, fibers were transferred to 1× phosphate buffered saline (PBS, Gibco) for at least 10 min before spectra were assessed. Functionalized fibers can be stored long-term in clean plastic or glassware.

Production of Covalently Modified nIRCats. SWNTs subjected to an aromatization reaction using cyanuric chloride and sodium azide can be solubilized in water via functionalization with ssDNA sequences without substantial loss of analyte-dependent fluorescence response.[34] We adapted the protocol described in Chio et al., 2020, to produce covalently modified nIRCats. In brief, pristine SWNTs were reacted with cyanuric chloride and sodium azide to produce TrZ-L-SWNT, which were subsequently reacted with ethylenediamine to produce NH_2-SWNT. $(GT)_6$-ssDNA was adsorbed to NH_2-SWNT as in Beyene et al., 2019, to yield NH_2-$(GT)_6$-SWNT, which was evaluated for DA response.

Covalent nIRCats-silica Linkage. *Triazine Functionalization.* Fibers were washed, etched, hydroxylated, and silanized as described above, then reacted with 1 g cyanuric chloride in 20 mL *N*-methyl-2-pyrrolidone (NMP) at 70 °C for 24 h to produce triazine-functionalized silica fibers. Triazine-functionalized fibers were then incubated in an aqueous solution of NH_2-$(GT)_6$-SWNT for 24 h.

1,3,5-Tris(bromomethyl)benzene Functionalization. Fibers were washed, etched, hydroxylated, and silanized as described above, then reacted with 20 mL dimethylformamide, 250 μL triethylamine, and 250 mg TBMB at 70 °C for 24 h under nitrogen. Fibers were then incubated in a solution of NH_2-$(GT)_6$-SWNT for 24 h.

Exchange of SWNT Solvents. *Chemical Desiccation.* In brief, nIRCats prepared as in Beyene et al., 2019 or NH_2-$(GT)_6$-SWNT as described above were combined with a water-miscible polar aprotic solvent, then a desiccant was added to remove water. 50 μL each of acetone, dimethylformamide (DMF), dimethyl sulfoxide (DMSO), and NMP, and were added to separate aliquots of 50 μL nIRCat solution, then agitated. 50 μL solvent was subsequently added with agitation between each addition until the total volume of solution reached 250 μL. Approximately 100 mg anhydrous sodium sulfate was added and solutions were stored at 10 °C.

Evaporation and Reconstitution. nIRCats prepared as in Beyene et al., 2019 or NH_2-$(GT)_6$-SWNT as described above were evaporated under reduced pressure, then the resulting residue was vigorously agitated with water or with polar aprotic solvents. 250 μL aqueous SWNT solution was added to a 50 mL round-bottom flask and the water was removed under reduced pressure using a rotary evaporator. 250 μL of water, NMP, or DMSO was added, and the

https://doi.org/10.1021/acs.langmuir.4c04910
Langmuir XXXX, XXX, XXX−XXX

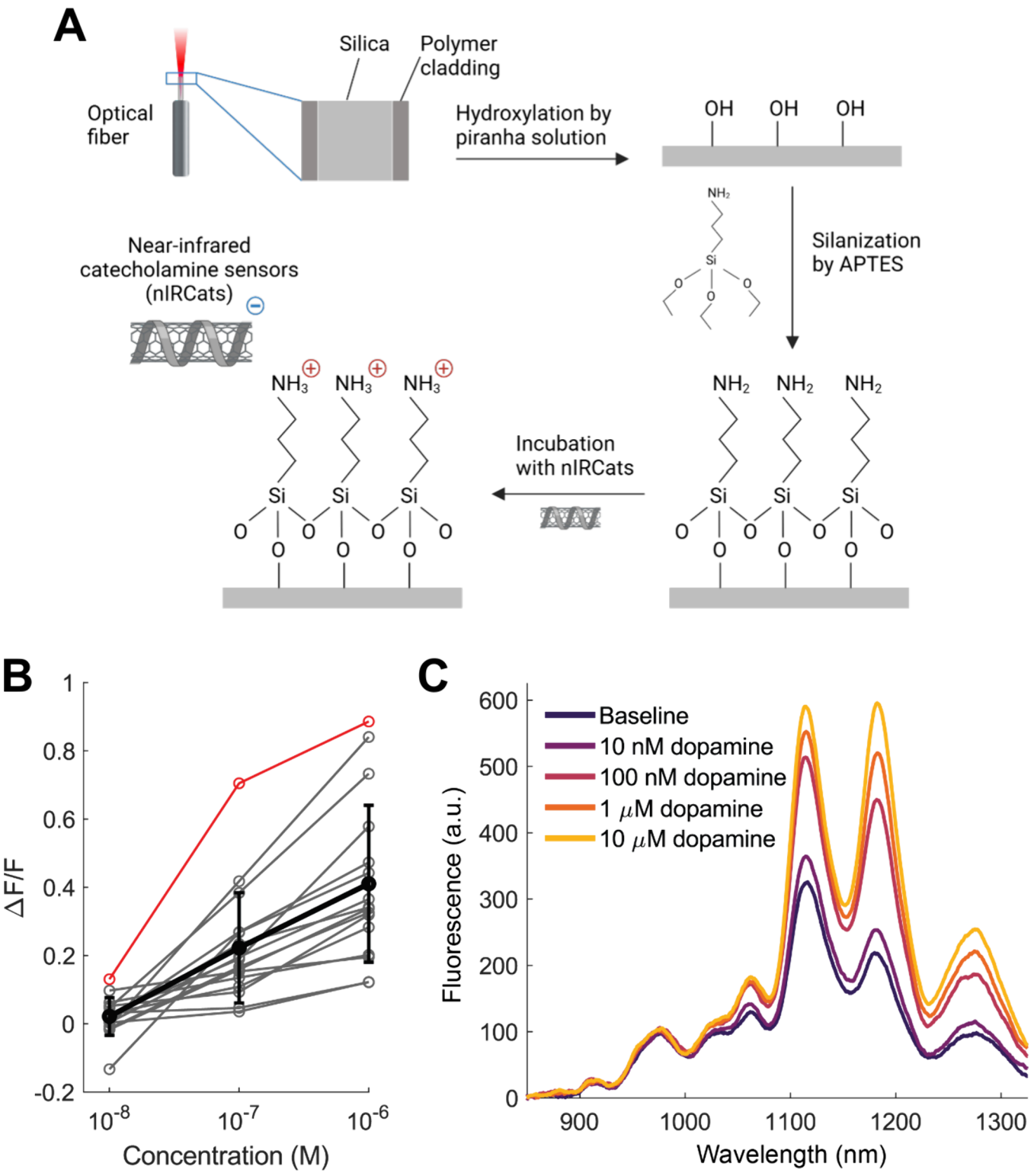

Figure 1. (A) Schematic representation of silica surface functionalization. The optical fibers used in this study consist of a silica core and a hard polymer cladding (FP400URT, Thorlabs). The silica surface is optionally first hydroxylated using a piranha solution, followed by silanization with APTES. The functionalized fibers are then incubated with near-infrared catecholamine nanosensors (nIRCats), promoting electrostatic interactions between the negatively charged nIRCats and the aminosilane groups on the silica surface. Further details on the functionalization procedure are provided in the Experimental Section. (B) Integrated fluorescence from 1050 to 1300 nm for increasing concentrations of dopamine for individual functional fibers (gray lines, n = 16) and mean (black line; error bars = SD). (C) Representative spectra from one fiber (red in panel B) in 1× PBS and in increasing concentrations of dopamine *in vitro*..

residue was agitated under the solvent. The solvent was collected and centrifuged at 2 × 10^4 rcf for 30 min at room temperature, and the supernatant was collected and characterized by UV−vis absorbance and IR fluorescence spectroscopy. An approximate extinction coefficient for SWNT in DMSO at 632 nm was calculated by serial dilution of known-concentration aqueous NH_2-$(GT)_6$-SWNT in

https://doi.org/10.1021/acs.langmuir.4c04910
Langmuir XXXX, XXX, XXX−XXX

DMSO followed by averaging the calculated values. This value was then used to approximate the concentration of SWNT in DMSO.

Laser/Spectrometer Data Collection. A 721 nm laser (Opto Engine LLC) was fiber-coupled to an inverted Zeiss microscope (Axio Observer D1). A 60 cm-long sheathed fiber with a plastic ferrule at one end was coupled directly to the light source in place of an objective and provided a conduit for excitation light. Each individual nIRF fiber was then plugged into the plastic ferrule at the end of the conduit fiber; laser power exiting the fiber was measured to be 4−8 mW. Each nIRF fiber was suspended in 40 mL 1× PBS. Fluorescence spectra were collected from 850 to 1300 nm by a Princeton Instruments spectrograph (SCT 320) and a liquid nitrogen-cooled Princeton Instruments InGaAs linear array detector (PyLoN-IR). Each fiber was equilibrated to the solution and laser light for 10 min in 1× PBS with the microscope shutter open before baseline spectrum collection. Thereafter, a 1 mM DA solution was added directly into the PBS in increments of 0.4 μL, 4 μL, 40 μL, and 400 μL to produce 10 nM, 100 nM, 1 μM, and 10 μM DA solutions, respectively, unless otherwise noted. Spectra were collected 1 min after each subsequent addition of DA. When assessing spectra in small volumes, fibers were suspended in individual 10 μL aliquots of 10 nM, 100 nM, and 1 μM DA. Fibers were equilibrated for 10 min in each solution before data was acquired.

Solutions. *Artificial Cerebrospinal Fluid (aCSF).* aCSF was prepared in-house, consisting of sodium chloride (6.90 g/L), potassium chloride (0.26 g/L), hydrated magnesium chloride (0.264 g/L), sodium phosphate (0.12 g/L), sodium bicarbonate (2.20 g/L), D-glucose (1.98 g/L), and hydrated calcium chloride (0.37 g/L) in one liter of Milli-Q water.

Brain Homogenate. The brain of one adult male mouse was extracted in accordance with laboratory animal care guidelines. 5 mL 1× PBS was immediately added to the brain and homogenate was generated by probe-tip sonication for 30 min.

Blood Plasma. Frozen 1 mL aliquots of human blood plasma (pooled, Lee Biosciences) were thawed and diluted with 1× PBS.

Acute Slice Preparation. Slices were obtained from C57BL/6 adult male mice. Mice were group-housed after weaning at postnatal day 21 (P21) and kept with nesting material on a 12:12 light cycle. All animal procedures were approved by the University of California Berkeley Animal Care and Use Committee. Acute brain slices were prepared using established protocols.[28,29] Briefly, mice were deeply anesthetized via intraperitoneal injection of ketamine/xylazine cocktail, and transcardial perfusion was performed using ice-cold cutting buffer (119 mM NaCl, 26.2 mM $NaHCO_3$, 2.5 mM KCl, 1 mM NaH_2PO_4, 3.5 mM $MgCl_2$, 10 mM glucose, and 0 mM $CaCl_2$), after which the brain was rapidly extracted. The cerebellum and other connective tissues were trimmed using a razor blade, and the brain was mounted onto the cutting stage of a vibratome (Leica VT1200 S). 300 μm thick slices including the dorsal striatum were prepared. Slices were incubated at 37 °C for 60 min in oxygen-saturated ACSF (119 mM NaCl, 26.2 mM $NaHCO_3$, 2.5 mM KCl, 1 mM NaH_2PO_4, 1.3 mM $MgCl_2$, 10 mM glucose, and 2 mM $CaCl_2$) before use.

Dual-nIR Fiber Photometry Rig and Electrical Stimulation. We designed and constructed a mobile dual-nIR fiber photometry rig for use with nIRF fibers in *ex vivo* and *in vivo* applications. A 635 nm excitation laser (35−50 mW at end of conduit fiber) was fiber coupled, collimated, and deflected into a patch fiber by a 900 nm long-pass dichroic mirror. The patch fiber allows for individual nIRF fibers to be implanted in tissue and connected when needed via a plastic sleeve. Emission light from nIRF fibers travels through the same patch fiber and passes through the dichroic mirror to an ultrasensitive, thermoregulated nIR camera (Ninox 640 II, Raptor Photonics). The patch fiber was affixed to the camera lens such that the only light entering the lens was from the fiber itself. For each acquisition, Micro-Manager imaging software (v. 1.4.23) acquired 600 frames at 8.33 Hz with 0.5 mA electrical stimulation triggered at frame 200. All nIRF fibers used on this rig are first evaluated for *in vitro* DA response with the spectrometer.

Analysis of Fluorescence. For spectroscopic data, we integrated fluorescence values (arbitrary units) from 1050 to 1300 nm for all readings. Each fiber's fluorescence in 1× PBS served as the baseline against which subsequent measurements from that fiber were normalized. For nIR camera images, image acquisition was controlled by Micro-Manager software, which summed pixel intensity from a 640 × 512 pixel field of view, an area which encapsulated the totality of the 400 μm-diameter nIRF fiber surface. A line fit between the average of the first 50 frames and average of the last 50 frames of each acquisition was taken as the fluorescence baseline to correct for drift; all fluorescence values are represented normalized relative to that baseline. All analysis was performed in MATLAB using custom scripts.

RESULTS AND DISCUSSION

We developed a protocol for aminosilane-based immobilization[33] of nIRCats on glass optical fibers. 400 μm diameter multimode silica optical fibers were cleaned, then silanized with 5% (3-aminopropyl)triethoxysilane (APTES) solution in toluene. After overnight curing at 110 °C, fibers were passively incubated in nIRCat solution to promote an electrostatic interaction between the DNA adsorbed on the SWNT backbone and the aminosilane bound to the silica of the fiber (Figure 1A and Figure S1). This electrostatic interaction increased the number of nIRCats immobilized on the silica surface (Figure S2). The surface coverage was confirmed by a near-infrared fluorescent microscope (Figure S3). We first assessed the fluorescent spectra of these nIRCat-functionalized (nIRF) fibers in a 40 mL solution of 1× phosphate buffered saline (PBS) to approximate saline conditions of biological environments. In agreement with the known dopamine response of solution-phase nIRCat,[28,35] we observed a response profile with characteristic peaks at 1150 and 1200 nm from all fibers. To assess the functionality of immobilized nIRCats, we added aliquots of concentrated dopamine solution directly to the PBS solution to produce sequential solutions of 10 nM, 100 nM, and 1 μM dopamine. To enforce a standard of quality control, we rejected any fiber that exhibited $\Delta F/F_0 <$ 0.1 to 1 μM dopamine as nonfunctional (Figure S4). As with solution-phase nIRCat (Figure S5), we observed a stepwise increase in fluorescent response above baseline fluorescence, $\Delta F/F_0$, to each subsequent addition of dopamine in 16/21 fibers, though the individual response magnitude varied between the 16 functional replicates (10 nM dopamine = 0.022 ± 0.056 $\Delta F/F_0$, 100 nM dopamine = 0.223 ± 0.162 $\Delta F/F_0$, and 1 μM dopamine = 0.411 ± 0.230 $\Delta F/F_0$ (means ± SD); n = 16; $P < 0.001$ between 10 nM versus 100 nM dopamine and $P = 0.015$ between 100 nM versus 1 μM dopamine, two-tailed t test; Figure 1B,C).

To assess the reversibility of functional fibers and the impact of potential biofouling by molecules present in biological environments,[36] we assessed a new batch of fibers (n = 6) in dopamine, rinsed them in 1× PBS, then incubated them in 10× diluted human blood plasma overnight (>16 h). After incubation, we observed comparable responses to dopamine (before incubation: 10 nM dopamine = 0.036 ± 0.050 $\Delta F/F_0$, 100 nM dopamine = 0.271 ± 0.202 $\Delta F/F_0$, and 1 μM dopamine = 0.390 ± 0.242 $\Delta F/F$; after incubation: 10 nM dopamine = 0.033 ± 0.025 $\Delta F/F_0$, 100 nM dopamine = 0.198 ± 0.118 $\Delta F/F$, and 1 μM dopamine = 0.381 ± 0.189 $\Delta F/F_0$; P = 0.623 between time points, repeated-measures ANOVA; Figure 2A), indicating that our fibers are both reusable and robust to blood plasma exposure. As blood plasma contains only a small subset of biomolecules present in the living brain, we next sought to test performance in an extreme biological environment containing a high level of potential bioconta-

https://doi.org/10.1021/acs.langmuir.4c04910
Langmuir XXXX, XXX, XXX−XXX

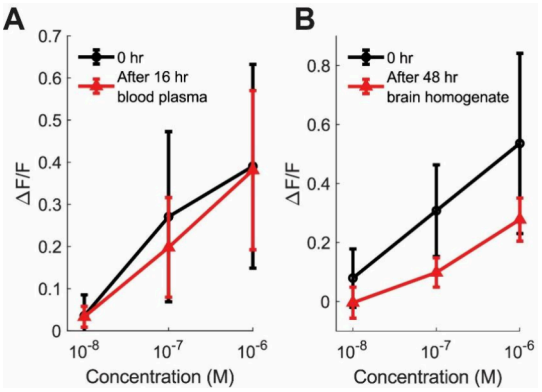

Figure 2. Average nIRF fluorescent responses to increasing concentrations of dopamine (error bars = SD; n = 6). (A) Before plasma incubation (black) vs after overnight plasma incubation (red). (B) Before brain homogenate incubation (black) vs after 48 h brain homogenate incubation (red).

minants. We pretested and then incubated a new batch of fibers (n = 4) in brain homogenate solution for 48 h and observed a noticeable, but not statistically significant, attenuation of response (before incubation: 10 nM dopamine = 0.080 ± 0.099 $\Delta F/F_0$, 100 nM dopamine = 0.308 ± 0.156 $\Delta F/F_0$, and 1 μM dopamine = 0.536 ± 0.306 $\Delta F/F_0$; after incubation: 10 nM dopamine = −0.004 ± 0.053 $\Delta F/F_0$, 100 nM dopamine = 0.098 ± 0.050 $\Delta F/F_0$, and 1 μM dopamine = 0.278 ± 0.073 $\Delta F/F_0$; P = 0.222 between time points, repeated-measures ANOVA; Figure 2B), indicating that even in this extreme case, nIRF fibers are not completely defunctionalized by biocontaminants.

To examine the longevity of nIRF fibers and their use in a broader range of biological environments, we prepared a new batch of fibers (n = 4) for long-term dry storage. After 24 weeks, despite a nearly 50% reduction in baseline fluorescence, nIRF fibers could reliably detect dopamine without a statistically significant attenuation in fluorescent response relative to the initial performance (date of manufacture: 10 nM dopamine = 0.002 ± 0.020 $\Delta F/F_0$, 100 nM dopamine = 0.414 ± 0.378 $\Delta F/F_0$, and 1 μM dopamine = 0.687 ± 0.355 $\Delta F/F_0$; after 24 weeks: 10 nM dopamine = 0.024 ± 0.053 $\Delta F/F_0$, 100 nM dopamine = 0.266 ± 0.174 $\Delta F/F_0$, and 1 μM dopamine = 0.517 ± 0.235 $\Delta F/F_0$; P = 0.479 between time points, repeated-measures ANOVA; Figure 3A,B). Despite a slight attenuation of fluorescence, 24-week-old fibers maintained a biologically relevant response range for potential *in vivo* applications (10−100 nM dopamine). These data suggest nIRF fibers are shelf-stable, reusable, and generate repeatable results, ideal for experimental or clinical applications.

We next sought to explore the utility of nIRF fibers in another potential clinical application: biofluid samples commonly used in diagnostic testing. To this end, we tested these same 24-week-old fibers in artificial cerebrospinal fluid (aCSF) and 100× diluted human blood plasma. While heretofore, tests had been performed in 40 mL solution to enable sequential increases in dopamine concentration, we modified our protocol to assess nIRF fiber performance in as little as 10 μL volume to account for the reduced clinical availability of patient biofluids. In all biofluid solutions, though baseline fluorescence was attenuated compared to the baseline in 1× PBS on the manufacturing date, responses to 10 nM dopamine were comparable to 10 nM dopamine in 1× PBS as summarized in Table 1 (P = 0.872 between 40 mL 1× PBS versus 40 mL blood plasma, P = 0.344 between 40 mL 1× PBS versus 40 mL aCSF, P = 0.394 between 40 mL aCSF versus 10 μL aCSF, all repeated-measures ANOVA; Figure 3A,B, further detail in Table S1).

As further proof of principle, we assessed the response of one fiber in 10 μL undiluted blood plasma. Compared to initial performance in PBS, this fiber exhibited a greater response to dopamine in undiluted human blood plasma after 24 weeks, with 0.182 $\Delta F/F_0$, 0.221 $\Delta F/F_0$, and 0.856 $\Delta F/F_0$ to 10 nM, 100 nM, and 1 μM dopamine, respectively (Figure 3C). Taken together, these data show that nIRF fibers can detect dopamine in small volumes of human biofluids, supporting the clinical utility of nIRF fibers in indicating potential risk factors for complex human disease.

We then targeted detection of evoked dopamine release from *ex vivo* dorsal striatum, an area of the brain densely innervated by dopaminergic fibers. While endogenous dopamine release in the mouse dorsal striatum in response to reward in the intact brain ranges from about 1−20 nM,[37] electrically evoked dopamine in the same region can extend into the micromolar range,[38] well within the detection range of nIRF fibers. We constructed a compact, mobile dual-nIR fiber photometry rig with a 635 nm excitation laser, ultrasensitive thermoregulated nIR camera (Ninox 640, Raptor Photonics),

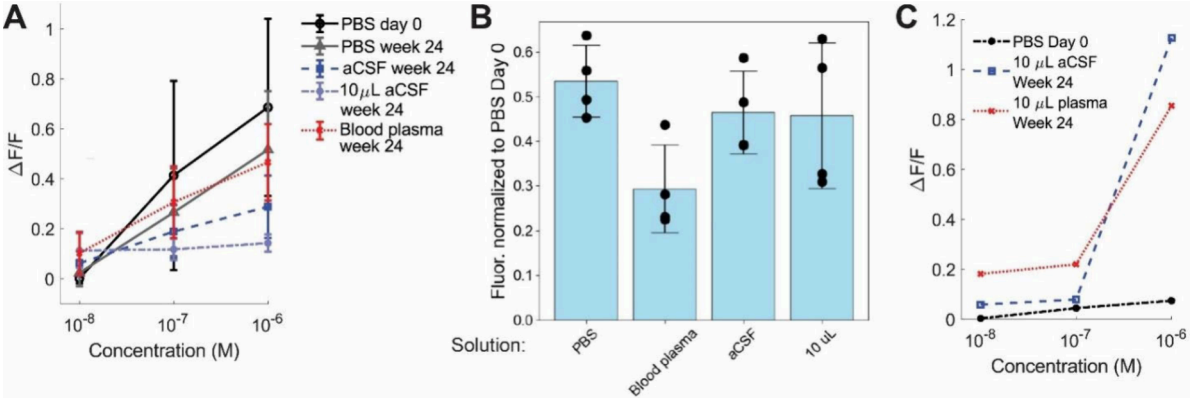

Figure 3. (A) Average nIRF fiber response in biologically relevant solutions (n = 4; error bars = SD). (B) Baseline fluorescence after 24 weeks in tested solutions relative to baseline fluorescence in 1× PBS on manufacturing date (circles = individual fibers, error bars = SD). (C) Single fiber response profile in clinically relevant solution volumes.

https://doi.org/10.1021/acs.langmuir.4c04910
Langmuir XXXX, XXX, XXX−XXX

Table 1. Fluorescent Responses to Dopamine in Different Media

Solvent	40 mL 1× PBS	40 mL diluted blood plasma	40 mL aCSF	10 μL aCSF
10 nM dopamine	0.024 ± 0.053	0.103 ± 0.086	0.063 ± 0.048	0.114 ± 0.069
100 nM dopamine	0.266 ± 0.174	0.307 ± 0.143	0.190 ± 0.106	0.118 ± 0.043
1 μM dopamine	0.517 ± 0.235	0.467 ± 0.152	0.289 ± 0.126	0.143 ± 0.035

and flexible patch cord (Figure 4A) and prepared 300 μm-thick slices of mouse striatum in a bath continually perfused with

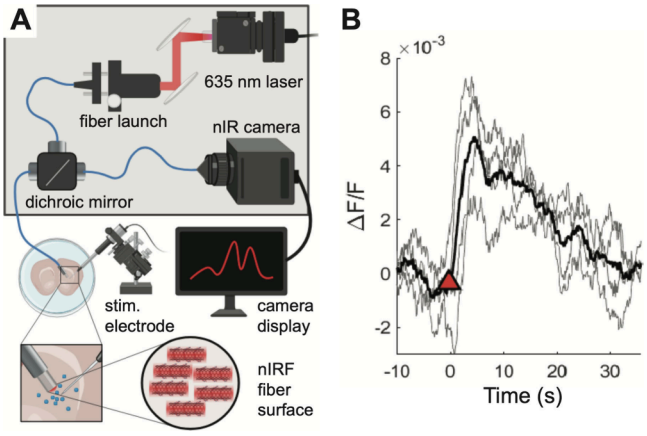

Figure 4. (A) Schematic of 12″ × 18″ breadboard-based fiber photometry rig compatible with other recording platforms. (B) Baseline-corrected fluorescent response to electrically evoked DA release in excised brain tissue. Gray traces correspond to individual trials (n = 4, one fiber); black = average; red triangle indicates time of stimulation.

aCSF, as in previous work with solution-phase nIRCats.[28,29] We implanted a platinum iridium stimulating electrode and a nIRF fiber in the same slice and recorded a small but consistent increase in fluorescence corresponding to stimulation over four consecutive trials (mean peak $\Delta F/F_0$ = 0.005), providing evidence of endogenous dopamine release from *ex vivo* brain tissue (Figure 4B). This experiment further serves as a proof of principle that, despite attenuation of signal after exposure to brain tissue, dopamine detection within a biological environment is feasible with nIRF fibers.

While we observed consistent responses from most nIRF fibers, we also observed that some fibers were nonresponsive to dopamine, which we attributed to the variable availability or accessibility of silanol groups for nIRCat bonding on the fiber surface. We thus tested protocol modifications (summarized in Table S2) toward the goal of regularizing fiber output. To promote greater availability of silanol groups, we treated fibers with a base bath of potassium hydroxide in ethanol and then hydroxylated the silica surface in a solution of concentrated sulfuric acid and 30% hydrogen peroxide (piranha solution). Finally, we bath sonicated fibers in nIRCat solution to facilitate interaction between nIRCats and the fiber surface. These protocol modifications increased the average baseline fluorescent response nearly 4-fold relative to the originally described protocol (P = 0.0012, Wilcoxon ranked sum test); this greater density of bound nIRCats, however, yielded a reduction in fluorescent response to dopamine in comparison to our standard protocol (P = 0.022 significant effect of protocol, two-way ANOVA, Figure S6). We hypothesize that the dynamic range of the functionalized fibers may have an inherent maximum dictated by the fiber architecture rather than functionalization density. Furthermore, the dynamic range of fluorescent response to dopamine may be attenuated by steric overcrowding of nIRCats immobilized on the fiber surface.

We next considered whether a covalent interaction between SWNT and silica might promote a greater density of dopamine-responsive nIRCats on the fiber surface, as a single nanotube could occupy several amine sites on the silanized silica surface through our standard protocol.[39] Moreover, localized pH changes in a physiological environment could potentially desorb ssDNA from SWNT,[40] thus disrupting the nIRCat-silica bond. Certain covalent bonds, however, may be less susceptible to pH fluctuation-related cleavage. To this end, we assessed the performance of fibers functionalized with covalently modified SWNTs, which have been shown to maintain analyte-dependent fluorescence responses.[34] We prepared aromatized SWNTs (NH_2-$(GT)_6$-SWNT) as in Chio et al., 2020, then silanized fibers as described followed by the addition of cyanuric chloride to produce triazine-functionalized silica fibers, which were reacted with aromatized nIRCats to covalently link nIRCats to the fibers. This modification yielded fibers with consistent dopamine response but weaker baseline signal (n = 6; baseline fluorescence significantly lower than standard protocol, P < 0.001, Wilcoxon ranked-sum; no significant effect of protocol on dopamine response, P = 0.317, two-way ANOVA; Figure S7). We subsequently introduced a 1,3,5-tris(bromomethyl)-benzene (TBMB) reaction, commonly used in the cross-linking of complex polymers,[41] in attempt to produce a silica surface functionalized with reactive bromo-substituted benzylic carbons before reacting the fiber with aromatized SWNTs. This modification yielded fibers with well-quenched fluorescent baselines exhibiting a characteristic SWNT profile (n = 5; baseline fluorescence significantly lower than standard protocol, P = 0.001, Wilcoxon ranked-sum) and moderate dopamine response, but no improvement of signal compared to our previous electrostatic SWNT-silane manufacturing protocol (no significant effect of protocol on dopamine response, P = 0.156, two-way ANOVA; Figure S6).

As nIRCat solution is prepared in water, we sought to assess the effect of solution nucleophilicity on fiber performance by exploring alternative SWNT solution solvents. We desiccated standard aqueous aromatized SWNT solution through rotary evaporation, then attempted to reconstitute the residue separately in four polar aprotic solvents: acetone, dimethylformamide (DMF), dimethyl-sulfoxide (DMSO), and *N*-methyl-pyrrolidone (NMP). Reconstitution was successful only with DMSO. Triazine-functionalized fibers incubated in DMSO-SWNT solution yielded baseline fluorescence spectra that were indistinguishable from our standard preparation (P = 0.971, Wilcoxon signed-rank) but did not demonstrate the expected fluorescence response to dopamine (significant effect of protocol and significant interaction between protocol and dopamine response, both P < 0.001, two-way ANOVA; Figure S6). Together, these experiments provide further insight into

https://doi.org/10.1021/acs.langmuir.4c04910
Langmuir XXXX, XXX, XXX−XXX

the nature of functionalized SWNTs in hydrous and anhydrous environments, in solution and immobilized form.

In their current form, nIRF fibers serve as proof of principle turnkey, shelf-stable, reversible, reusable probes for detection of dopamine at nanomolar levels in small volumes of biofluids. Though fibers exhibit substantial variability in detection, this is common among engineered biosensors and can be overcome by screening and calibrating fiber fluorescence in known concentrations of dopamine prior to use in experimental or clinical samples. We foresee a unique advantage of this tool, upon further development, in the realm of clinical evaluations of catecholamine levels in biofluids such as blood, cerebrospinal fluid, and urine. While blood plasma contains dopamine at subnanomolar concentrations,[42] norepinephrine is present at 1.5−1.8 nM.[43] CSF contains dopamine at 1.3−21.7 nM[12,44] and norephinephrine at up to 25 nM,[12,45] and urine contains dopamine at 65−400 μg/24h[46] and norepinephrine at 15−80 μg/24h.[47] Elevated plasma and CSF dopamine levels in the 10 nM range are associated with certain pathologies, including coronary artery disease[48] and psychosis.[49,50] These concentrations are within the dynamic range detectable by nIRF fibers. There is a growing interest in improved biosensors for clinical catecholamine detection from lower-volume samples,[51−55] and we have demonstrated that nIRF fibers can detect dopamine in as little as 10 μL of sample. Moreover, because our sensor platform does not require the addition of subsequent reagents, nIRF fibers permit reversible catecholamine detection in patient samples, which can then be reused for subsequent assays, reducing the overall volume of sample needed in diagnostic testing. Taken together, these attributes elevate nIRF fibers as a promising first-pass diagnostic tool.

Additionally, our work contributes to a greater understanding of SWNT fluorescent dynamics in a unique fiber form factor. We have demonstrated that baseline fluorescence is not necessarily indicative of dopamine detection sensitivity; fibers with low baseline fluorescence perform just as well, if not better than, higher-baseline fibers (Figures 4, S3). Indeed, prior work has shown that low initial baseline fluorescence of nIRCat dopamine sensors enables larger dopamine-specific responses, and it is possible this phenomenon extends to our nIRF fibers as well.[34,56] Conversely, covalently linking SWNTs to the silica surface of the fiber failed to amplify dopamine response, which we postulate could be due to unintended reactions between the halide-functionalized silica and nucleotides in the ssDNA oligomer or pH-driven desorption.

One limitation of this tool is the apparent attenuation of fluorescence observed after long-term exposure to brain homogenate. This could be due to biofouling compromising the exciton recombination efficiency of nIRCats or endonucleases compromising the integrity of the $(GT)_6$ functionalization on nIRCat surfaces. Previous work has identified biofouling via the SWNT protein corona as a prominent source of nanosensor attenuation.[57] Future work to combat biofouling may explore passivation of SWNTs with polyethylene glycol, which reduces SWNT-induced platelet aggregation,[58] permits circulation *in vivo*,[27] improves targeted drug delivery success,[59] minimizes cytotoxicity and nonspecific cellular interactions,[60] reduces expression of inflammatory cytokines, attenuates microglial activation, and further enhances dopamine imaging.[35] An alternative approach to nIRF fiber synthesis could encapsulate nIRCats in a hydrogel, which has demonstrated excellent biocompatibility and light-guiding properties.[32,61] This strategy has successfully enabled SWNT-based sensors for detection of steroid hormones,[62] essential vitamins,[63] and chemotherapeutic drugs[64] *in vivo*. Moreover, this strategy has recently proved applicable to large mammal models for multiweek sensing without adverse health effects,[65] suggesting tractability across species. Further investigation combining these strategies may present a viable route by which to successfully utilize nIRCats in living brain tissue.

CONCLUSION

In summary, we developed catecholamine-sensitive, near-infrared nanosensor-functionalized optical (nIRF) fibers and a compatible dual-nIR mobile fiber photometry imaging platform to readily detect extracellular dopamine *in vitro* and *ex vivo*. We have demonstrated that this tool can be successfully used to detect signals up to 24 weeks postproduction and is robust to biofouling anticipated with chronic implantation in biological tissue. This form factor introduces the possibility of real-time extracellular catecholamine imaging, potentially permitting a broader range of time-sensitive studies across multiple species with fewer invasive procedures. Overall, we foresee this tool as a starting point from which to expand resources available for quickly assessing biofluid catecholamine levels, chronic catecholamine monitoring in genetically intractable or time-sensitive model systems, or and study of the effects of catecholamine pharmacology. These data represent the first step in development of a turnkey optical probe for catecholamine detection that may provide a real-time readout of catecholamine release during human surgery or the ability to chronically monitor catecholamine levels in a patient over time, leading to a deeper understanding of the catecholamine dynamics behind the progression and treatment of debilitating human illnesses.

ASSOCIATED CONTENT

Data Availability Statement

All raw data and processing and analysis code are available upon request.

Supporting Information

The Supporting Information is available free of charge at https://pubs.acs.org/doi/10.1021/acs.langmuir.4c04910.

Figure S1 showing photograph of prepared fiber to scale and in dopamine detection; Figure S2 showing fluorescence spectra from silanized fibers and non-silanized fibers.; Figure S3 showing surface coverage characterization by a near-infrared fluorescent microscope.; Figure S4 showing fluorescent responses of nonfunctional fibers to increasing concentrations of dopamine; Figure S5 showing fluorescent spectra of nIRCat nanosensors in solution form; Figure S6 showing demonstration of baseline fluorescence and dopamine response due to protocol modifications; Figure S7 showing demonstration of baseline fluorescence and dopamine response from alternative protocols; Table S1 listing summarized experiment responses to dopamine; Table S2 listing results of modifications to standard nIRF fiber preparation protocol (PDF)

https://doi.org/10.1021/acs.langmuir.4c04910
Langmuir XXXX, XXX, XXX−XXX

AUTHOR INFORMATION

Corresponding Author

Markita P. Landry − *Helen Wills Neuroscience Institute, Department of Chemical and Biomolecular Engineering, and California Institute for Quantitative Biosciences, University of California Berkeley, Berkeley, California 94720, United States; Innovative Genomics Institute, Berkeley, California 94720, United States; Chan Zuckerberg Biohub, San Francisco, California 94063, United States;* orcid.org/0000-0002-5832-8522; Email: landry@berkeley.edu

Authors

Madeline E. Klinger − *Helen Wills Neuroscience Institute, University of California Berkeley, Berkeley, California 94720, United States;* orcid.org/0000-0003-0866-5325

Rigney A. Miller − *College of Chemistry, University of California Berkeley, Berkeley, California 94720, United States*

Natsumi Komatsu − *Department of Chemical and Biomolecular Engineering, University of California Berkeley, Berkeley, California 94720, United States*

Amanda Shiu − *Department of Chemical and Biomolecular Engineering, University of California Berkeley, Berkeley, California 94720, United States*

Linda Wilbrecht − *Helen Wills Neuroscience Institute and Department of Psychology, University of California Berkeley, Berkeley, California 94720, United States*

Complete contact information is available at: https://pubs.acs.org/10.1021/acs.langmuir.4c04910

Author Contributions

Project was conceived by M.P.L. and L.W. All authors contributed to experiment design. M.E.K. performed all experiments except protocol modification experiments, which were performed by R.A.M., N.K., and A.S. M.E.K. analyzed all data. M.E.K. wrote most of the manuscript with contributions from R.A.M, M.P.L., and L.W. All authors edited and approved the final manuscript.

Funding

We acknowledge support of a Burroughs Wellcome Fund Career Award at the Scientific Interface (CASI) (M.P.L. and N.K.), a Dreyfus Foundation Award (MPL), the Philomathia Foundation (MPL), an NIH MIRA Award R35GM128922 (M.P.L.), an NIH R21 NIDA Award 1R03DA052810 (M.P.L.), an NIH R21 NIDA Award R21DA044010 (to L.W. and M.P.L.), an NSF CAREER Award 2046159 (M.P.L.), an NSF CBET Award 1733575 (to M.P.L.), a CZI Imaging Award (M.P.L.), a Sloan Foundation Award (M.P.L.), a McKnight Foundation Award (M.P.L.), a Simons Foundation Award (M.P.L.), a Moore Foundation Award (M.P.L.), a Schmidt Foundation Award (M.P.L.), and Schmidt Science Fellows (N.K.). M.P.L. is a Chan Zuckerberg Biohub Investigator and a Hellen Wills Neuroscience Institute Investigator.

Notes

The authors declare no competing financial interest.

ACKNOWLEDGMENTS

We thank J. Travis Del Bonis-O'Donnell, Ph.D., for feedback and direction regarding silanization and M. Moein Safaee, Ph.D., for assistance constructing the fiber photometry rig.

REFERENCES

(1) Ungerstedt, U. Adipsia and Aphagia after 6-Hydroxydopamine Induced Degeneration of the Nigro-Striatal Dopamine System. *Acta Physiol. Scand.* **1971**, *82* (S367), 95−122.

(2) Schultz, W. Predictive Reward Signal of Dopamine Neurons. *J. Neurophysiol.* **1998**, *80* (1), 1−27.

(3) Murray, A. M.; Weihmueller, F. B.; Marshall, J. F.; Hurtig, H. I.; Gottleib, G. L.; Joyce, J. N. Damage to Dopamine Systems Differs between Parkinson's Disease and Alzheimer's Disease with Parkinsonism. *Ann. Neurol.* **1995**, *37* (3), 300−312.

(4) Martorana, A.; Koch, G. Is Dopamine Involved in Alzheimer's Disease? *Front. Aging Neurosci.* **2014**, *6*, 252.

(5) Grace, A. A. Dysregulation of the Dopamine System in the Pathophysiology of Schizophrenia and Depression. *Nat. Rev. Neurosci.* **2016**, *17* (8), 524−532.

(6) Basu, S.; Dasgupta, P. S. Dopamine, a Neurotransmitter, Influences the Immune System. *J. Neuroimmunol.* **2000**, *102* (2), 113−124.

(7) Jose, P. A.; Eisner, G. M.; Felder, R. A. Regulation of Blood Pressure by Dopamine Receptors. *Nephron Physiol.* **2003**, *95* (2), 19−27.

(8) Mignini, F.; Streccioni, V.; Amenta, F. Autonomic Innervation of Immune Organs and Neuroimmune Modulation. *Auton. Autacoid Pharmacol.* **2003**, *23* (1), 1−25.

(9) Rubí, B.; Maechler, P. Minireview: New Roles for Peripheral Dopamine on Metabolic Control and Tumor Growth: Let's Seek the Balance. *Endocrinology* **2010**, *151* (12), 5570−5581.

(10) Lambert, G.; Johansson, M.; Agren, H.; Friberg, P. Reduced Brain Norepinephrine and Dopamine Release in Treatment-Refractory Depressive Illness: Evidence in Support of the Catecholamine Hypothesis of Mood Disorders. *Arch. Gen. Psychiatry* **2000**, *57* (8), 787−793.

(11) Rommelfanger, K. S.; Weinshenker, D. Norepinephrine: The Redheaded Stepchild of Parkinson's Disease. *Biochem. Pharmacol.* **2007**, *74* (2), 177−190.

(12) Henjum, K.; Watne, L. O.; Godang, K.; Halaas, N. B.; Eldholm, R. S.; Blennow, K.; Zetterberg, H.; Saltvedt, I.; Bollerslev, J.; Knapskog, A. B. Cerebrospinal Fluid Catecholamines in Alzheimer's Disease Patients with and without Biological Disease. *Transl. Psychiatry* **2022**, *12* (1), 151.

(13) Berridge, C. W.; Schmeichel, B. E.; España, R. A. Noradrenergic Modulation of Wakefulness/Arousal. *Sleep Med. Rev.* **2012**, *16* (2), 187−197.

(14) Grella, S. L.; Gomes, S. M.; Lackie, R. E.; Renda, B.; Marrone, D. F. Norepinephrine as a Spatial Memory Reset Signal. *Behav. Pharmacol.* **2021**, *32* (7), 531−548.

(15) Tank, A. W.; Lee Wong, D. Peripheral and Central Effects of Circulating Catecholamines. *Compr. Physiol.* **2015**, *5* (1), 1−15.

(16) Devoto, P.; Flore, G.; Pani, L.; Gessa, G. L. Evidence for Co-Release of Noradrenaline and Dopamine from Noradrenergic Neurons in the Cerebral Cortex. *Mol. Psychiatry* **2001**, *6* (6), 657−664.

(17) Sánchez-Soto, M.; Bonifazi, A.; Cai, N. S.; Ellenberger, M. P.; Newman, A. H.; Ferré, S.; Yano, H. Evidence for Noncanonical Neurotransmitter Activation: Norepinephrine as a Dopamine D2-Like Receptor Agonist. *Mol. Pharmacol.* **2016**, *89* (4), 457−466.

(18) Xing, B.; Li, Y.-C.; Gao, W.-J. Norepinephrine versus Dopamine and Their Interaction in Modulating Synaptic Function in the Prefrontal Cortex. *Brain Res.* **2016**, *1641* (Part B), 217−233.

(19) Ranjbar-Slamloo, Y.; Fazlali, Z. Dopamine and Noradrenaline in the Brain; Overlapping or Dissociate Functions? *Front. Mol. Neurosci.* **2020**, *12*, 334.

(20) Post, M. R.; Sulzer, D. The Chemical Tools for Imaging Dopamine Release. *Cell Chem. Biol.* **2021**, *28* (6), 748−764.

(21) Kruss, S.; Hilmer, A. J.; Zhang, J.; Reuel, N. F.; Mu, B.; Strano, M. S. Carbon Nanotubes as Optical Biomedical Sensors. *Adv. Drug Delivery Rev.* **2013**, *65* (15), 1933−1950.

(22) Jain, A.; Homayoun, A.; Bannister, C. W.; Yum, K. Single-Walled Carbon Nanotubes as near-Infrared Optical Biosensors for Life Sciences and Biomedicine. *Biotechnol. J.* **2015**, *10* (3), 447−459.
(23) Hendler-Neumark, A.; Bisker, G. Fluorescent Single-Walled Carbon Nanotubes for Protein Detection. *Sensors* **2019**, *19* (24), 5403.
(24) Smith, A. M.; Mancini, M. C.; Nie, S. Bioimaging: Second Window for in Vivo Imaging. *Nat. Nanotechnol.* **2009**, *4* (11), 710−711.
(25) Li, Z.; de Barros, A. L. B.; Soares, D. C. F.; Moss, S. N.; Alisaraie, L. Functionalized Single-Walled Carbon Nanotubes: Cellular Uptake, Biodistribution and Applications in Drug Delivery. *Int. J. Pharm.* **2017**, *524* (1), 41−54.
(26) Galassi, T. V.; Antman-Passig, M.; Yaari, Z.; Jessurun, J.; Schwartz, R. E.; Heller, D. A. Long-Term in Vivo Biocompatibility of Single-Walled Carbon Nanotubes. *PloS One* **2020**, *15* (5), No. e0226791.
(27) Iverson, N. M.; Barone, P. W.; Shandell, M.; Trudel, L. J.; Sen, S.; Sen, F.; Ivanov, V.; Atolia, E.; Farias, E.; McNicholas, T. P.; Reuel, N.; Parry, N. M. A.; Wogan, G. N.; Strano, M. S. In Vivo Biosensing via Tissue-Localizable near-Infrared-Fluorescent Single-Walled Carbon Nanotubes. *Nat. Nanotechnol.* **2013**, *8* (11), 873−880.
(28) Beyene, A. G.; Delevich, K.; Del Bonis-O'Donnell, J. T.; Piekarski, D. J.; Lin, W. C.; Thomas, A. W.; Yang, S. J.; Kosillo, P.; Yang, D.; Prounis, G. S.; Wilbrecht, L.; Landry, M. P. Imaging Striatal Dopamine Release Using a Nongenetically Encoded near Infrared Fluorescent Catecholamine Nanosensor. *Sci. Adv.* **2019**, *5* (7), No. eaaw3108.
(29) Yang, S. J.; O'Donnell, J. T.; del, B.; Giordani, F.; Wang, J.; Lui, A.; Piekarski, D.; Irrinki, A.; Schaffer, D. V.; Landry, M. P. Synaptic Scale Dopamine Disruption in Huntington's Disease Model Mice Imaged with near Infrared Catecholamine Nanosensors. *bioRxiv* **2022**, DOI: 10.1101/2022.09.19.508617.
(30) Elizarova, S.; Chouaib, A. A.; Shaib, A.; Hill, B.; Mann, F.; Brose, N.; Kruss, S.; Daniel, J. A. A Fluorescent Nanosensor Paint Detects Dopamine Release at Axonal Varicosities with High Spatiotemporal Resolution. *Proc. Natl. Acad. Sci. U. S. A.* **2022**, *119* (22), No. e2202842119.
(31) Bulumulla, C.; Krasley, A. T.; Cristofori-Armstrong, B.; Valinsky, W. C.; Walpita, D.; Ackerman, D.; Clapham, D. E.; Beyene, A. G. Visualizing Synaptic Dopamine Efflux with a 2D Composite Nanofilm. *eLife* **2022**, *11*, No. e78773.
(32) Kozawa, D.; Cho, S. Y.; Gong, X.; Nguyen, F. T.; Jin, X.; Lee, M. A.; Lee, H.; Zeng, A.; Xue, G.; Schacherl, J.; Gibson, S.; Vega, L.; Strano, M. S. A Fiber Optic Interface Coupled to Nanosensors: Applications to Protein Aggregation and Organic Molecule Quantification. *ACS Nano* **2020**, *14* (8), 10141−10152.
(33) Zhu, M.; Lerum, M. Z.; Chen, W. How to Prepare Reproducible, Homogeneous, and Hydrolytically Stable Aminosilane-Derived Layers on Silica. *Langmuir ACS J. Surf. Colloids* **2012**, *28* (1), 416−423.
(34) Chio, L.; Pinals, R. L.; Murali, A.; Goh, N. S.; Landry, M. P. Covalent Surface Modification Effects on Single-Walled Carbon Nanotubes for Targeted Sensing and Optical Imaging. *Adv. Funct. Mater.* **2020**, *30* (17), No. 1910556.
(35) Beyene, A. G.; Alizadehmojarad, A. A.; Dorlhiac, G.; Goh, N.; Streets, A. M.; Král, P.; Vuković, L.; Landry, M. P. Ultralarge Modulation of Fluorescence by Neuromodulators in Carbon Nanotubes Functionalized with Self-Assembled Oligonucleotide Rings. *Nano Lett.* **2018**, *18* (11), 6995−7003.
(36) Yang, D.; Yang, S. J.; Del Bonis-O'Donnell, J. T.; Pinals, R. L.; Landry, M. P. Mitigation of Carbon Nanotube Neurosensor Induced Transcriptomic and Morphological Changes in Mouse Microglia with Surface Passivation. *ACS Nano* **2020**, *14* (10), 13794−13805.
(37) Natori, S.; Yoshimi, K.; Takahashi, T.; Kagohashi, M.; Oyama, G.; Shimo, Y.; Hattori, N.; Kitazawa, S. Subsecond Reward-Related Dopamine Release in the Mouse Dorsal Striatum. *Neurosci. Res.* **2009**, *63* (4), 267−272.
(38) Taylor, I. M.; Nesbitt, K. M.; Walters, S. H.; Varner, E. L.; Shu, Z.; Bartlow, K. M.; Jaquins-Gerstl, A. S.; Michael, A. C. Kinetic Diversity of Dopamine Transmission in the Dorsal Striatum. *J. Neurochem.* **2015**, *133* (4), 522−531.
(39) Nimse, S. B.; Song, K.; Sonawane, M. D.; Sayyed, D. R.; Kim, T. Immobilization Techniques for Microarray: Challenges and Applications. *Sensors* **2014**, *14* (12), 22208−22229.
(40) Shearer, C. J.; Yu, L.; Fenati, R.; Sibley, A. J.; Quinton, J. S.; Gibson, C. T.; Ellis, A. V.; Andersson, G. G.; Shapter, J. G. Adsorption and Desorption of Single-Stranded DNA from Single-Walled Carbon Nanotubes. *Chem.—Asian J.* **2017**, *12* (13), 1625−1634.
(41) Yang, J.; Jiang, H.; Gao, L.; Wang, J.; Xu, Y.; He, R. Fabrication of Crosslinked Polybenzimidazole Membranes by Trifunctional Crosslinkers for High Temperature Proton Exchange Membrane Fuel Cells. *Int. J. Hydrog. Energy* **2018**, *43* (6), 3299−3307.
(42) Gardner, D. G.; Shoback, D. Appendix: Normal Hormone Reference Ranges. In *Greenspan's Basic & Clinical Endocrinology*; The McGraw-Hill Companies: New York, NY, 2011.
(43) Goldstein, D. S.; Holmes, C. Neuronal Source of Plasma Dopamine. *Clin. Chem.* **2008**, *54* (11), 1864−1871.
(44) Scheinin, M.; Seppala, T.; Koulu, M.; Linnoila, M. Determination of Conjugated Dopamine in Cerebrospinal Fluid from Humans and Non-Human Primates with High Performance Liquid Chromatography Using Electrochemical Detection. *Acta Pharmacol. Toxicol. (Copenh.)* **1984**, *55* (2), 88−94.
(45) Goldstein, D. S.; Holmes, C.; Sharabi, Y. Cerebrospinal Fluid Biomarkers of Central Catecholamine Deficiency in Parkinson's Disease and Other Synucleinopathies. *Brain J. Neurol* **2012**, *135* (6), 1900−1913.
(46) Pagana, K. D.; Pagana, T. J.; Pagana, T. N. *Mosby's Diagnostic and Laboratory Test Reference*, 12th ed.; Elsevier: Saint Louis, MO, 2015.
(47) Hollstein, T.; Basolo, A.; Ando, T.; Votruba, S. B.; Krakoff, J.; Piaggi, P. Urinary Norepinephrine Is a Metabolic Determinant of 24-Hour Energy Expenditure and Sleeping Metabolic Rate in Adult Humans. *J. Clin. Endocrinol. Metab.* **2020**, *105* (4), 1145−1156.
(48) Abe, M.; Iwaoka, M.; Nakamura, T.; Kitta, Y.; Takano, H.; Kodama, Y.; Kawabata, K.; Obata, J.; Mende, A.; Kobayashi, T.; Fujioka, D.; Saito, Y.; Hasebe, H.; Kugiyama, K. Association of High Levels of Plasma Free Dopamine with Future Coronary Events in Patients with Coronary Artery Disease. *Circ. J. Off. J. Jpn. Circ. Soc.* **2007**, *71* (5), 688−692.
(49) Takase, M.; Kimura, H.; Kanahara, N.; Nakata, Y.; Iyo, M. Plasma Monoamines Change under Dopamine Supersensitivity Psychosis in Patients with Schizophrenia: A Comparison with First-Episode Psychosis. *J. Psychopharmacol. Oxf. Engl* **2020**, *34* (5), 540−547.
(50) Orhan, F.; Goiny, M.; Becklén, M.; Mathé, L.; Piehl, F.; Schwieler, L.; Fatouros-Bergman, H.; Farde, L.; Cervenka, S.; Sellgren, C. M.; Engberg, G.; Erhardt, S. CSF Dopamine Is Elevated in First-Episode Psychosis and Associates to Symptom Severity and Cognitive Performance. *Schizophr. Res.* **2023**, *257*, 34−40.
(51) Zhang, K.; Liu, Y.; Wang, Y.; Zhang, R.; Liu, J.; Wei, J.; Qian, H.; Qian, K.; Chen, R.; Liu, B. Quantitative SERS Detection of Dopamine in Cerebrospinal Fluid by Dual-Recognition-Induced Hot Spot Generation. *ACS Appl. Mater. Interfaces* **2018**, *10* (18), 15388−15394.
(52) Shi, Y.; Pang, Y.; Huang, N.; Sun, C.; Pan, Y.; Cheng, Y.; Long, Y.; Zheng, H. Competitive Method for Fluorescent Dopamine Detection in Cerebrospinal Fluid Based on the Peroxidase-like Activity of Ficin. *Spectrochim. Acta. A. Mol. Biomol. Spectrosc.* **2019**, *209*, 8−13.
(53) Senel, M.; Dervisevic, E.; Alhassen, S.; Dervisevic, M.; Alachkar, A.; Cadarso, V. J.; Voelcker, N. H. Microfluidic Electrochemical Sensor for Cerebrospinal Fluid and Blood Dopamine Detection in a Mouse Model of Parkinson's Disease. *Anal. Chem.* **2020**, *92* (18), 12347−12355.

https://doi.org/10.1021/acs.langmuir.4c04910
Langmuir XXXX, XXX, XXX−XXX

(54) Nawrot, W.; Drzozga, K.; Baluta, S.; Cabaj, J.; Malecha, K. A Fluorescent Biosensors for Detection Vital Body Fluids' Agents. *Sensors* **2018**, *18* (8), 2357.
(55) Ravariu, C. From Enzymatic Dopamine Biosensors to OECT Biosensors of Dopamine. *Biosensors* **2023**, *13* (8), 806.
(56) Alizadehmojarad, A. A.; Zhou, X.; Beyene, A. G.; Chacon, K. E.; Sung, Y.; Pinals, R. L.; Landry, M. P.; Vuković, L. Binding Affinity and Conformational Preferences Influence Kinetic Stability of Short Oligonucleotides on Carbon Nanotubes. *Adv. Mater. Interfaces* **2020**, *7* (15), No. 2000353.
(57) Pinals, R. L.; Yang, D.; Rosenberg, D. J.; Chaudhary, T.; Crothers, A. R.; Iavarone, A. T.; Hammel, M.; Landry, M. P. Quantitative Protein Corona Composition and Dynamics on Carbon Nanotubes in Biological Environments. *Angewandte Chemie (International ed. in English)* **2020**, *59* (52), 23668−23677.
(58) Sokolov, A. V.; Aseychev, A. V.; Kostevich, V. A.; Gusev, A. A.; Gusev, S. A.; Vlasova, I. I. Functionalization of Single-Walled Carbon Nanotubes Regulates Their Effect on Hemostasis. *J. Phys. Conf. Ser.* **2011**, *291*, No. 012054.
(59) Al Faraj, A.; Shaik, A. S.; Ratemi, E.; Halwani, R. Combination of Drug-Conjugated SWCNT Nanocarriers for Efficient Therapy of Cancer Stem Cells in a Breast Cancer Animal Model. *J. Controlled Release* **2016**, *225*, 240−251.
(60) Gao, Z.; Danné, N.; Godin, A. G.; Lounis, B.; Cognet, L. Evaluation of Different Single-Walled Carbon Nanotube Surface Coatings for Single-Particle Tracking Applications in Biological Environments. *Nanomaterials* **2017**, *7* (11), 393.
(61) Choi, M.; Choi, J. W.; Kim, S.; Nizamoglu, S.; Hahn, S. K.; Yun, S. H. Light-Guiding Hydrogels for Cell-Based Sensing and Optogenetic Synthesis in Vivo. *Nat. Photonics* **2013**, *7*, 987−994.
(62) Lee, M. A.; Wang, S.; Jin, X.; Bakh, N. A.; Nguyen, F. T.; Dong, J.; Silmore, K. S.; Gong, X.; Pham, C.; Jones, K. K.; Muthupalani, S.; Bisker, G.; Son, M.; Strano, M. S. Implantable Nanosensors for Human Steroid Hormone Sensing In Vivo Using a Self-Templating Corona Phase Molecular Recognition. *Adv. Healthc. Mater.* **2020**, *9* (21), No. e2000429.
(63) Bakh, N. A.; Gong, X.; Lee, M. A.; Jin, X.; Koman, V. B.; Park, M.; Nguyen, F. T.; Strano, M. S. Transcutaneous Measurement of Essential Vitamins Using Near-Infrared Fluorescent Single-Walled Carbon Nanotube Sensors. *Small Weinh. Bergstr. Ger.* **2021**, *17* (31), No. e2100540.
(64) Son, M.; Mehra, P.; Nguyen, F. T.; Jin, X.; Koman, V. B.; Gong, X.; Lee, M. A.; Bakh, N. A.; Strano, M. S. Molecular Recognition and In Vivo Detection of Temozolomide and 5-Aminoimidazole-4-Carboxamide for Glioblastoma Using Near-Infrared Fluorescent Carbon Nanotube Sensors. *ACS Nano* **2023**, *17* (1), 240−250.
(65) Hofferber, E.; Meier, J.; Herrera, N.; Stapleton, J.; Calkins, C.; Iverson, N. Detection of Single Walled Carbon Nanotube Based Sensors in a Large Mammal. *Nanomedicine Nanotechnol. Biol. Med.* **2022**, *40*, No. 102489.

https://doi.org/10.1021/acs.langmuir.4c04910
Langmuir XXXX, XXX, XXX−XXX